Article

Not peer-reviewed version

Au Nanoparticles Synthesis in the Presence of Thiolated Hyaluronic Acid

Lyudmila V. Parfenova *, Eliza I. Alibaeva, Guzel U. Gil'fanova, Zulfiya R. Galimshina, Ekaterina S. Mescheryakova, Leonard M. Khalilov, Semen N. Sergeev, Nikita V. Penkov, Challapalli Subrahmanyam

Posted Date: 7 October 2025

doi: 10.20944/preprints202510.0506.v1

Keywords: Au nanoparticles; Thiolated hyaluronic acid; Scanning transmission electron microscopy; Photon cross-correlation spectroscopy; X-ray photoelectron spectroscopy

 doi:10.20944/preprints202510.0506.v1

Article

Au Nanoparticles Synthesis in the Presence of Thiolated Hyaluronic Acid

Lyudmila V. Parfenova [1,*], Eliza I. Alibaeva [1], Guzel U. Gil'fanova [1], Zulfiya R. Galimshina [1], Ekaterina S. Mescheryakova [1], Leonard M. Khalilov [1], Semen N. Sergeev [2], Nikita V. Penkov [3] and Challapalli Subrahmanyam [4]

[1] Institute of Petrochemistry and Catalysis, Ufa Federal Research Center, Russian Academy of Sciences, Prosp. Oktyabrya, 141, 450075 Ufa, Russia

[2] Ufa University of Science and Technology, 12 Karl Marx Street, Ufa 450008, Russia

[3] Institute of Cell Biophysics of the Russian Academy of Sciences, Federal Research Center "Pushchino Scientific Center for Biological Research of the Russian Academy of Sciences", Institutskaya 3, 142290 Pushchino, Russia

[4] Department of Chemistry, Indian Institute of Technology Hyderabad, Kandi, Sangareddy 502284, Telangana, India

* Correspondence: luda_parfenova@mail.ru

Abstract

Gold nanoparticles (AuNPs) are of significant interest due to their unique properties and applications in biomedicine. While hyaluronic acid (HA) has been used to modify pre-formed AuNPs, its thiolated derivative (HA-SH) has been less explored for the direct synthesis and stabilization of AuNPs. This study investigates the use of thiolated hyaluronic acid as a key component in the synthesis of AuNPs. A series of HA-AuNPs (HA-AuNP1-4) were synthesized by reacting HA-SH with $HAuCl_4$ at different mass ratios. The resulting nanoparticles were characterized using UV-Vis spectroscopy, scanning/transmission electron microscopy (SEM/STEM), X-ray photoelectron spectroscopy (XPS), photon cross-correlation spectroscopy (PCCS), and zeta potential measurements. The chemical transformations of the thiol ligand were studied using NMR spectroscopy. The morphologies and sizes of AuNPs depended on the HA-SH to $HAuCl_4$ ratio, ranging from icosahedral and triangular particles (≥146 nm) to quasi-spherical particles with a bimodal distribution (6–7 nm and 45–60 nm). XPS confirmed the presence of metallic gold (Au^0) and Au-S bond, while NMR and XPS revealed the partial oxidation of thiol groups to sulfonic acid. Zeta potential measurements showed that lower $HAuCl_4$ concentrations resulted in higher negative charge (up to -41.5 mV), enhancing colloidal stability. This work demonstrates a versatile approach to the synthesis hyaluronic acid-based gold nanomaterials with tunable properties for potential biomedical applications.

Keywords: Au nanoparticles; Thiolated hyaluronic acid; Scanning transmission electron microscopy; Photon cross-correlation spectroscopy; X-ray photoelectron spectroscopy

1. Introduction

In recent decades, gold nanoparticles (AuNPs) have become the subject of a rapidly and exponentially growing number of studies. Due to their numerous beneficial properties, gold nanoparticles have secured a strong position in the global market. Gold nanoparticles are produced in a variety of forms and are characterized by large surface area, high electrical conductivity, bioinertness, stability, and excellent solubility. AuNPs are used in fields such as catalysis, optics, sensors, delivery of therapeutic agents, photodynamic therapy, and electronics [1–5].

Thus, the unique properties and high demand for AuNPs determine significant interest in these materials in scientific and practical fields. Fine-tuning the physical and chemical parameters of metal

 doi:10.20944/preprints202510.0506.v1

nanoparticles is possible due to advances in synthesis methods, which allow for variation in their composition, size, morphology, and stability.

The following three main reasons for the success of AuNPs are noted: (1) high chemical and physical stability, which also ensures biocompatibility, (2) ease of surface functionalization with organic and biological molecules, and (3) a variety of optical properties related to the presence of the surface plasmon resonance effect [6].

There are many methods for synthesizing AuNPs, which can be divided into two main classes: "top-down" or "bottom-up" [7]. "Bottom-up" transformations are of great interest because, by varying the nature of the precursor, reducing agent, stabilizer, and reaction conditions, it becomes possible to control the physical and chemical properties of the resulting nanoparticles.

The literature contains a substantial number of studies on the synthesis or use of AuNPs in the presence of various polysaccharides or the decoration of nanoparticles with polysaccharides [8–11]. Modification of inorganic components with polysaccharide – hyaluronic acid is used to develop materials employed in disease diagnostics, theranostics, drug delivery, and gene therapy [12]. Hyaluronic acid can be utilized as a reducing agent, as well as a stabilizing, non-fouling (antifouling), and biomolecule-targeting (biotargeting) ligand for nanoparticles [12]. For example, gold nanoparticles decorated with hyaluronic acid (HA) can serve as CD44-targeted anticancer agents [13]. AuNPs and thiol-modified biomacromonomers derived from hyaluronic acid (HA) and gelatin have been applied to form printable semisynthetic extracellular matrix (sECM) hydrogels [14]. The synthesis of AuNPs is known by the reaction of $HAuCl_4$ with hyaluronic acid (HA) [15], or in the presence of HA [16–19]. Dicarboxylated hyaluronate (DCH) and cellulose (DCC) with controlled composition and molecular weight have been used as reducing and stabilizing agents in an environmentally friendly one-step synthesis of AuNPs [20]. Thiolated hyaluronic acid has only been utilised as a modifier of pre-formed gold nanoparticles (AuNPs) [13,14,21,22].

The aim of this study is to explore the potential use of thiolated hyaluronic acid for the synthesis and stabilization of gold nanoparticles. The study investigated the transformation of HA-SH in reaction with $HAuCl_4$, the morphology, composition, size, and charge of the resulting gold particles.

2. Results and Discussion

2.1. HA-AuNP Synthesis

To obtain AuNPs, in the first stage, the synthesis of –S–S– and –SH derivatives of hyaluronic acid **1** and **2**, respectively, was carried out according to the method described in Refs. [23,24]. Using the polysaccharide, dithiodihydrazide, and the water-soluble dehydrating agent 1-ethyl-3-[3-(dimethylamino)propyl]carbodiimide (EDC) in a ratio of 2:1:1.5, the HA conjugate **1** was obtained with a substitution degree of approximately 40%. To obtain the HA derivative with terminal SH groups, the reducing agent DTT (dithiothreitol, Cleland's reagent) was added to the reaction mixture (Scheme 1). Compounds **1** (HA–S–S–HA) and **2** (HA–SH) were purified by dialysis. Next, compound **2** was reacted with $HAuCl_4$ at mass ratios of 1:(1–0.1) in bidistilled water, heated to 90 °C for 2 hours. Then, the mixture was left to stir at room temperature for 24 hours, resulting in a series of HA-AuNPs: [HA]:[$HAuCl_4$] = 1:0.25 (**HA-AuNP1**), 1:0.225 (**HA-AuNP2**), 1:0.20 (**HA-AuNP3**), 1:0.175 (**HA-AuNP4**).

 doi:10.20944/preprints202510.0506.v1

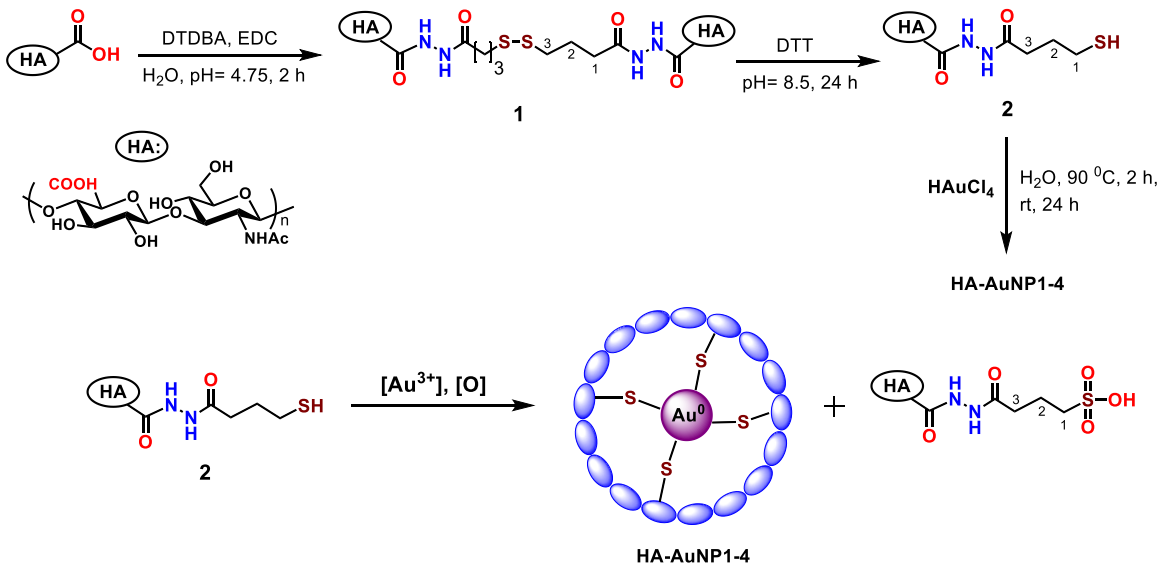

Scheme 1. Synthesis of **HA-AuNP1-4**

As shown in Figure 1, the color of the AuNP solutions gradually changed from yellow to violet-brown during the reaction, and from light violet to brown with increasing concentration of $HAuCl_4$.

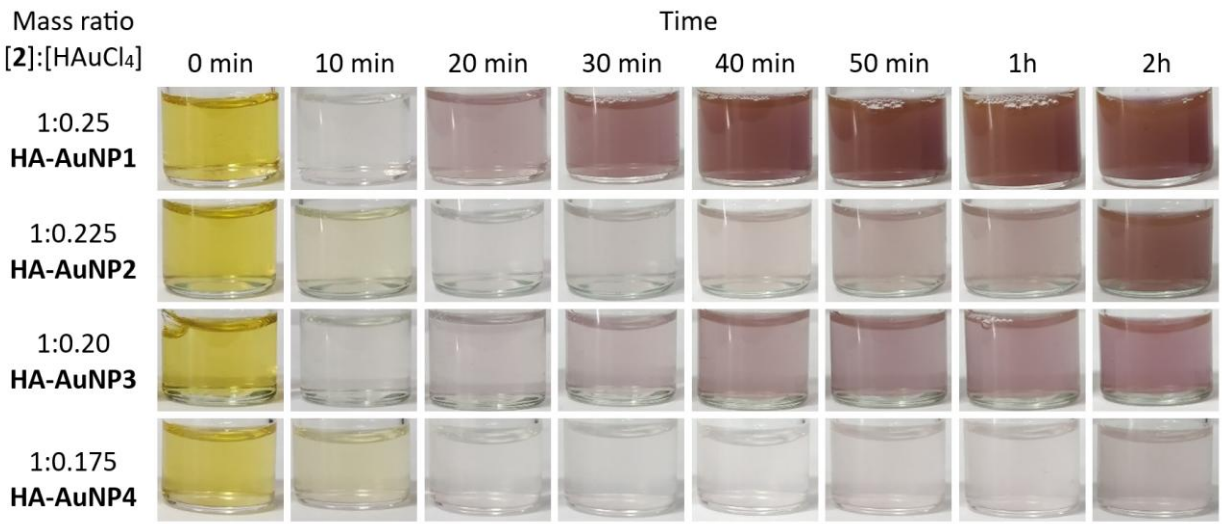

Figure 1. The color of solutions depending on time and the ratio of reagents **HA-AuNP1-4**.

2.2. HA-AuNP Characterization

The UV-visible absorption spectra of the **HA-AuNP1** to **HA-AuNP4** samples, shown in Figure 2, exhibited peaks in the range of 550–570 nm. This is characteristic of the surface plasmon resonance (SPR) of gold nanoparticles (AuNPs), which depends on their size, shape, and aggregation state [25–28].

The presence of a small peak in the UV spectrum for **AuNP4**, along with the pale violet color of the solution, may indicate a low concentration of particles, which is reflected in the decreased intensity.

 doi:10.20944/preprints202510.0506.v1

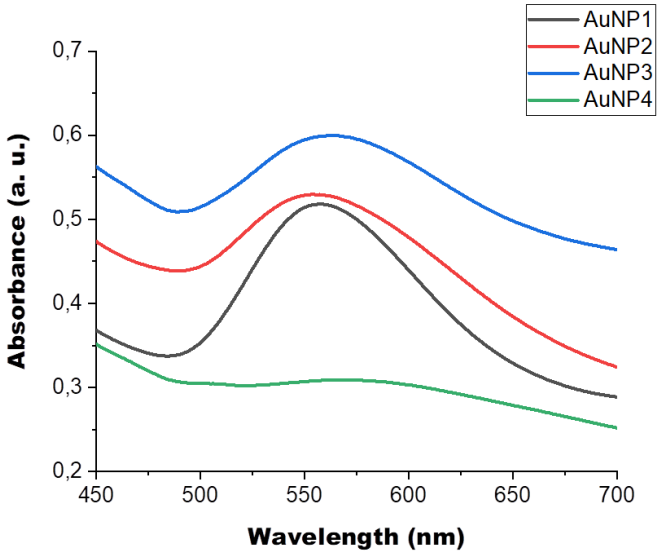

Figure 2. UV-Vis spectra of HA-AuNPs.

For further investigation of the morphology and structure of the samples, both scanning electron microscopy (SEM) and bright-field scanning transmission electron microscopy (BF-STEM) were used. These studies demonstrated that the shape and size of the particles depend on the synthesis conditions.

Figure 3 presents micrographs of **HA-AuNP1**, **HA-AuNP2**, and **HA-AuNP3**. SEM analysis confirmed that the synthesized particles are within the nanometer range and exhibit different morphologies depending on the concentration of $HAuCl_4$. The dark brown **HA-AuNP1** solution, as revealed by BF-STEM analysis, contains nanodisperse icosahedral particles measuring within the nanoscale (Figure 3b, Figure S4a-f), as well as equilateral triangular particles (Figure S4g-i) with sizes exceeding the nanometer range (diameter 146–172 nm). The particle size of **HA-AuNP1**, determined by PCCS, ranged from 65 to 90 nm (Figure S1). The icosahedral gold nanoparticles are surrounded by a modified hyaluronic acid shell with a thickness varying between 12 and 18 nm (Figure S4e).

In contrast, the **HA-AuNP2** solution consists exclusively of nanodisperse particles with heterogeneous shapes ranging from 40 to 70 nm (Figure 3c and Figure S5a-f). These AuNPs exhibit icosahedral, pentagonal, prismatic, trapezoidal, and triangular morphologies. Notably, hyaluronic acid forms a shell approximately 15 nm thick around smaller gold particles (~40 nm), while larger particles (60–70 nm) are coated with a shell measuring 15–20 nm in thickness (Figure S5d-f). PCCS size analysis showed particle diameters between 55 and 70 nm (Figure S2).

Unlike the previous two, the light violet **HA-AuNP3** solution contains only nanodisperse quasi-spherical particles enveloped by a polysaccharide shell, exhibiting a bimodal size distribution of 8–13 nm and around 50 nm (Figure 3e,f, Figure S6a-f). PCCS measurements also revealed a bimodal distribution for **HA-AuNP3** particles, with size populations centered at approximately 6–7 nm and 45–60 nm, respectively (Figure S3).

 doi:10.20944/preprints202510.0506.v1

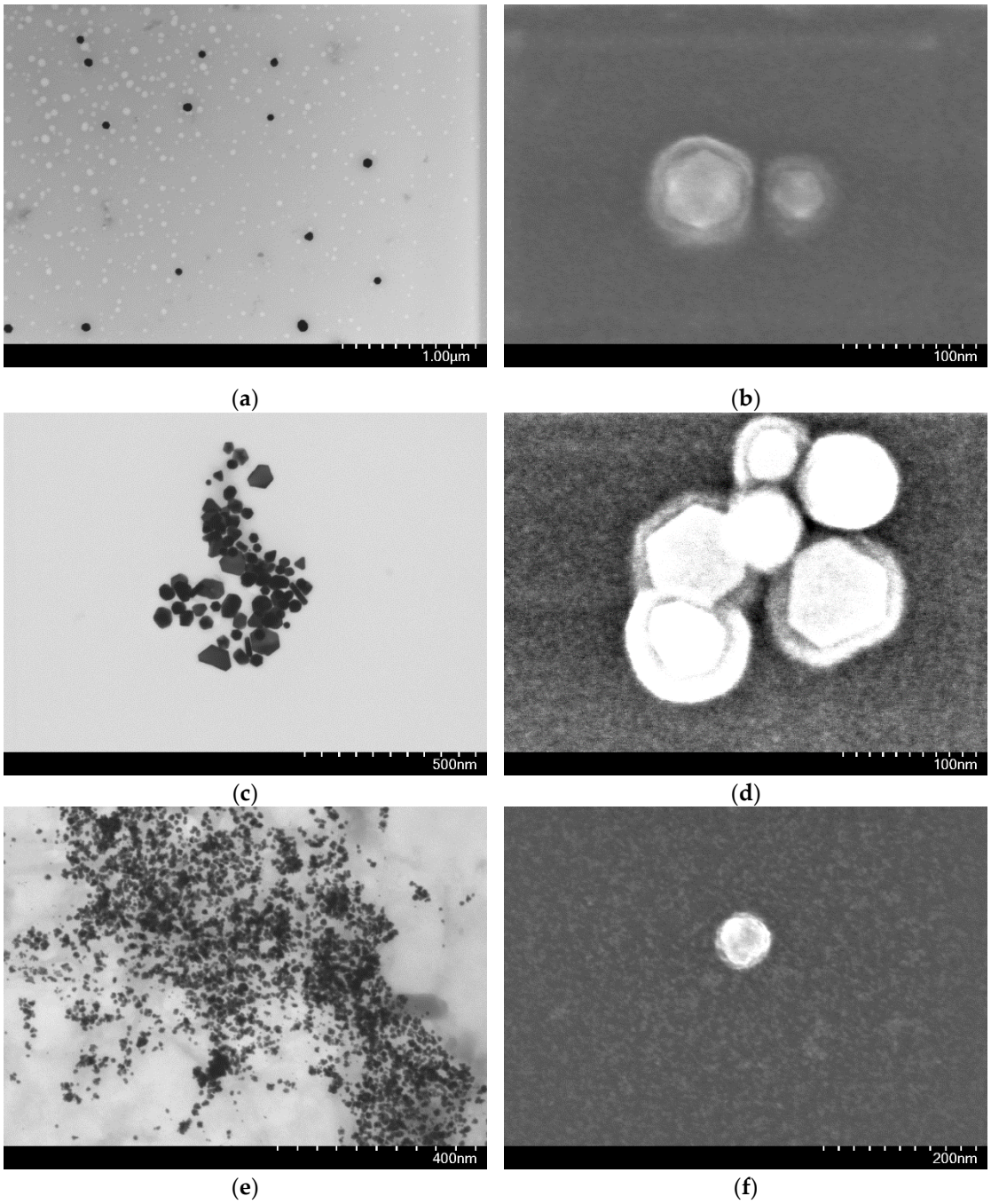

(a) (b) (c) (d) (e) (f)

Figure 3. BF-STEM and SEM images of AuNPs; microscopy characterization of precipitates at ×35 000 (**a**, **HA-AuNP1**), ×350 000 (**b**, **HA-AuNP1**), ×90 000 (**c**, **HA-AuNP2**), ×350 000 (**d**, **HA-AuNP2**), ×130 000 (**e**, **HA-AuNP3**), and ×200 000 (**f**, **HA-AuNP3**) magnifications (corresponding micrometer and nanometer scale bars shown on each image).

During the XPS analysis, the results of which are shown in Figure 4, it was demonstrated that the spectrum of the obtained **HA-AuNPs** (using **HA-AuNP3** as an example) is characterized by two main peaks Au 4f7/2 and Au 4f5/2 spin-orbit-splitting values of about 3.67 eV and a peak intensity ratio of 1.33, which is typical for gold [29–32]. The peak of Au at approximately 83.3 eV indicates the presence of Au^0, which is typical for nanoparticles with a preserved metallic structure [29–32]. The presence of the Au 4f(7/2) peak at a higher binding energy (83.8 eV) indicates the presence of an oxidized form of gold (Au(I)) [33].

The oxygen O1s is represented as three components: O1 532.3 (47.3%), O2 531.4 (27.4%), O3 529.6 (25.3%). The O1 peak at 532.3 eV can be attributed to the hydroxyl group [34,35]. The O2 component (531.4 eV) apparently corresponds to oxygen atoms of the amide bond, carboxylic group, or titanium

 doi:10.20944/preprints202510.0506.v1

hydroxide of the substrate. The O3 signal may belong to titanium oxide present on the metal substrate [36].

The XPS spectra contain two sulfur S2p signals at 168.1 eV and 162.9 eV. The peak at 162.9 eV corresponds to sulfide sulfur bound to the gold surface [37]. The peak at 168.1 eV may indicate a higher oxidation state of sulfur –SO_x–, which may point to the oxidation of disulfide/thiol ligands [38–41].

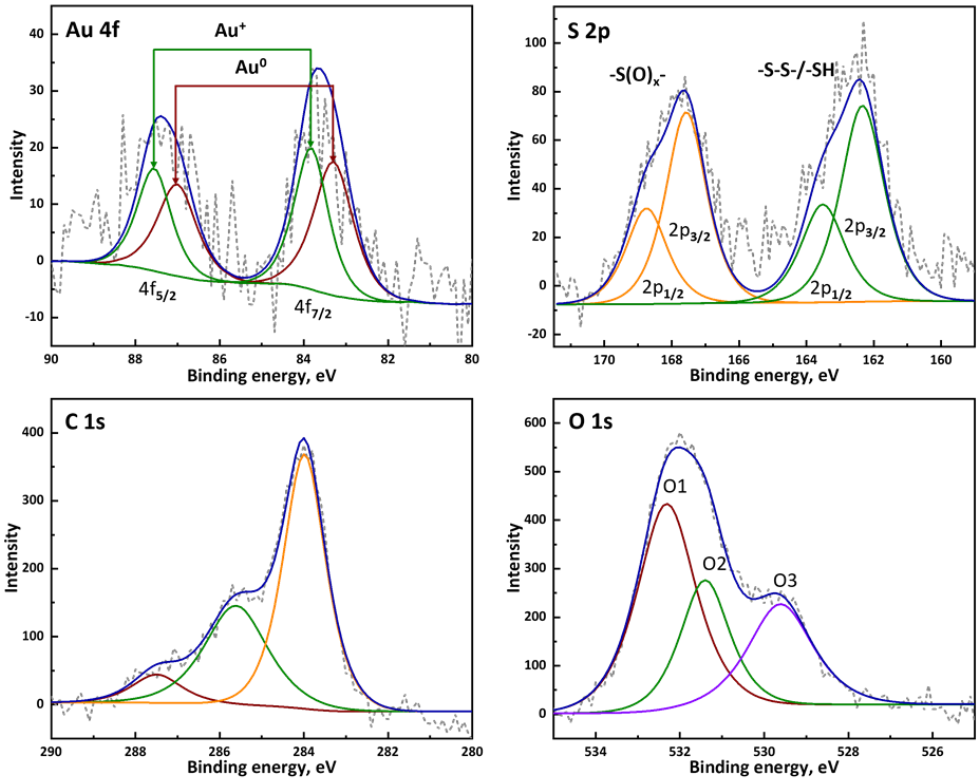

Figure 4. XPS spectra of **HA-AuNP3.**

Thus, as follows from the XPS spectra, the thiol group in the polysaccharide was partially oxidized to a sulfoxide, whose structure was clarified by us using NMR spectroscopy.

In the ^{1}H NMR spectrum of compound **1**, there is a broadened signal in the region δ 2.74 ppm, which corresponds to the protons of the methylene group at the -S-S- bond (-C$\underline{H}_2$-S-), and in the region δ_H 2.43 ppm related to the protons of the methylene group at C=O (Figure 5a). ^{1}H NMR spectrum of compound **2** exhibits a signal at δ_H 2.55 ppm, corresponding to the protons of the methylene group at the -SH bond (-C$\underline{H}_2$-SH), and δ_H 2.44 ppm, which relates to the methylene group at C=O (Figure 5b), while the resonance lines of hydrogen atoms at the C2 atom in both cases overlapped with the N-acetylmethyl protons of HA. The spectral data of compound **2** were consistent to the literature [42].

As indicated by the ^{1}H and ^{13}C NMR spectra of the reaction mixture obtained after the reaction of **2** with $HAuCl_4$, the thiol group undergoes significant changes, the result of which is apparently the formation of sulfonic acid. This is evidenced by the appearance of a new set of signals of –$(CH_2)_3$– fragments at δ_H 2.02 ppm, 2.43 ppm, and 2.89 ppm in the ^{1}H NMR spectra shifted to the downfield relative to the corresponding signals of compound **2** (Figure 5c). The intensity of these signals raised as the amount of $HAuCl_4$ introduced increased (Figure 5d). The multiplicity of the downfield signal of the protons of the CH_2 fragment at δ_H 2.89 corresponded to the pattern AA'BB' of the CH_2-CH_2 group (J_{AB}= 6.5, $J_{AB'}$= 9.0 Hz) with a predominance of the gauche conformation over the anti-conformation [43], which may be a consequence of the appearance of a symmetrical sulfonate group, limiting the conformational mobility of the hydrocarbon chain. The appearance of the sulfonate

 doi:10.20944/preprints202510.0506.v1

fragment is also indicated by the shift of the signal of the carbon atom at the sulfur atom from δ_C 23.03 ppm in compound **2** to δ_C 49.90 ppm (Figure S12) [44,45].

Thus, it can be assumed that along with the formation of AuNPs decorated with -S-HA, oxidation of the thiol group to sulfonic acid takes place, as represented in Scheme 1. The process apparently occurs with the participation of H_2O_2, the formation of which is possible as a result of the spontaneous reduction of Au^{3+} ions in $HAuCl_4$ solutions to Au^+ ions and Au nanoparticles [33], or with O_2. The interaction of HA-SH with Au^{3+} and hydrogen peroxide or oxygen can lead to cross-linking of the SH bonds with their transformation into HA-S-S-HA [46–48], and/or to the formation of sulfonic acid (Scheme 1) [49–51].

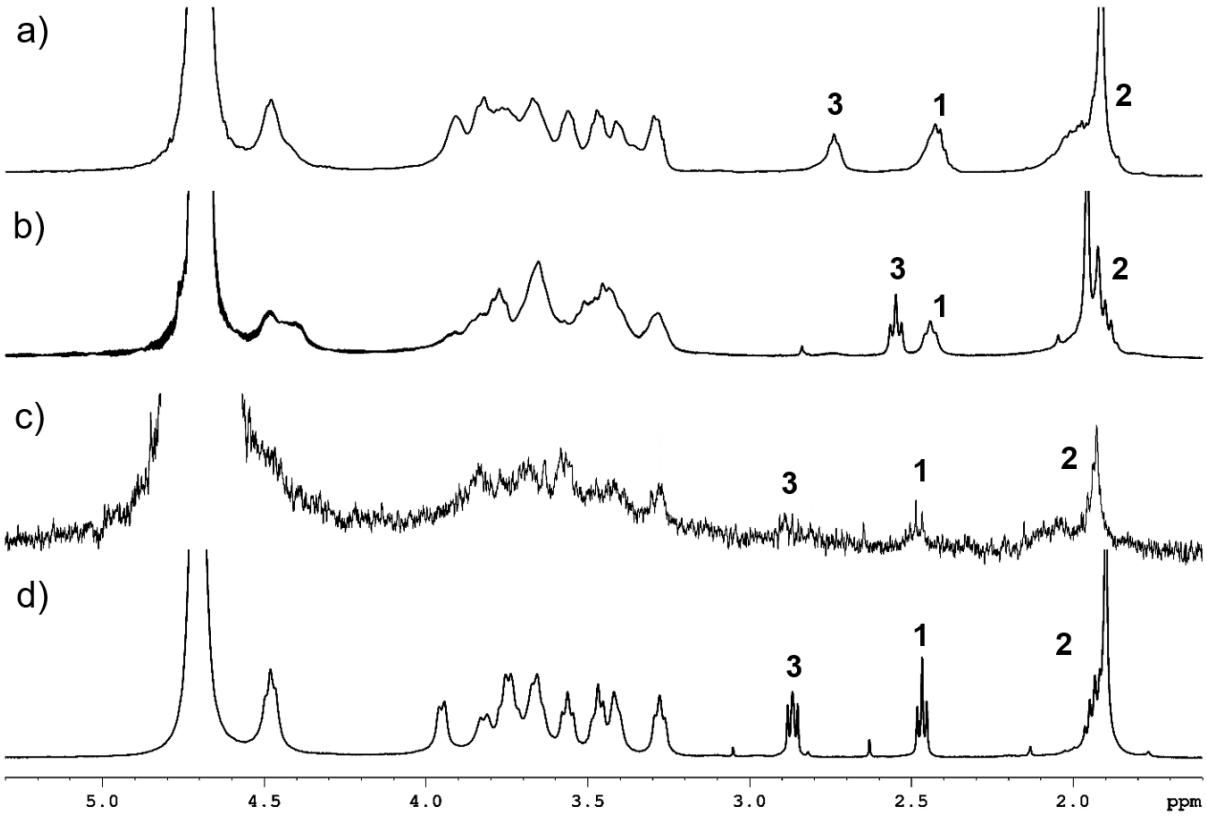

Figure 5. ^{1}H NMR spectra of compounds in D_2O: a) HA-S-S-HA (**1**); b) HA-SH (**2**); c) result of the reaction of **2** with $HAuCl_4$ at a ratio of [**2**]:[$HAuCl_4$]= 1:0.20; d) result of the reaction of **2** with $HAuCl_4$ at a ratio of [**2**]:[$HAuCl_4$]= 1:1.

To assess the electrostatic stability of colloidal systems, the ζ-potential was measured. The samples were analyzed in an aqueous medium at pH ~5-6 and room temperature. The obtained negative values of ζ-potential, presented in Table 1, indicate that AuNPs were coated with anionic HA [17]. AuNPs obtained at HA to $HAuCl_4$ ratios of 1:0.25 and 1:0.225 showed ζ-potential of –27.6 and –28.6 mV, respectively, whereas at lower Au concentrations of 1:0.20 and 1:0.175, a significant increase in negative charge to –41.0 and –41.5 mV, respectively, was observed, which indicates an increase in system stability [52,53]. The resulting sulfonic acid derivative of HA can also participate in the stabilization of gold nanoparticles.

Table 1. Values of ζ-potentials of samples **HA-AuNP1-4**.

	HA-AuNP1	**HA-AuNP2**	**HA-AuNP3**	**HA-AuNP4**
Zeta-potential (mV)	-27.6±3.4	-28.6±1.7	-41.0±4.0	-41.5±1.3

These data indicate that the use of different concentrations of $HAuCl_4$ affects the surface properties of the obtained AuNPs. Higher values of negative ζ-potential with decreasing amounts of

 doi:10.20944/preprints202510.0506.v1

$HAuCl_4$ may indicate more effective coating or stabilization of the nanoparticles by hyaluronic acid, which leads to an increase density of negatively charged functional groups on the surface. This contributes to an increase in electrostatic repulsion between particles, which in turn improves the stability of the system. On the other hand, at higher $HAuCl_4$ content (1:0.25 and 1:0.225), less negative values of ζ-potential are observed, which may be related to the partial neutralizing effect of gold ions or to a decrease in the availability of negatively charged HA groups on the nanoparticle surface. This can lead to a reduction in electrostatic stabilization and an increase in the probability of aggregation.

Thus, changing the ratio of thiol-modified HA to $HAuCl_4$ has a significant effect on the charge characteristics of the nanoparticle surface and, consequently, on their colloidal stability. Optimization of this parameter is a key factor for obtaining stable and functional nanomaterials based on hyaluronic acid and gold.

3. Materials and Methods

General Information. The following reagents were used for the synthesis: the low molecular weight (LMW) HA (<0.1 MDa), 4,4′-Dithiodibutyric acid (95%, Sigma Aldrich, Germany), 1-methyl-3-(3-dimethylaminopropyl)carbodiimide hydrochloride (EDC*HCl, 98%, ABCR, Germany), Cleland's Reagent (DTT, 98%, ABCR, Germany). 4,4′-Dithiodibutyric acid dihydrazide (DTDBA) was obtained by the method [54], SH-derivative of HA (**2**) was obtained according to the known procedure [42].

Spectroscopic studies were carried out by the means of ^{1}H and ^{13}C on an AVANCE-500 spectrometer (Bruker, operating frequency 500.17 MHz (^{1}H) and 125.78 MHz (^{13}C)). D_2O and $CDCl_3$ were used as internal standards and solvents. Samples were prepared in a standard ampoule with a diameter of 5 mm. The chemical shifts of hydrogen atoms are given in the scale δ (ppm) relative to tetramethylsilane (TMS). One- and two-dimensional NMR spectra (COSY ^{1}H–^{1}H, HSQC, HMBC, NOESY, DOSY) were recorded using standard Bruker pulse sequences.

Preparation of HA-AuNPs.

AuNPs were synthesized by the reaction of HA-SH (**2**) with $HAuCl_4$. Into an aqueous solution of HA-SH (**2**) with a concentration of 4.6 mg/ml under intensive stirring, an aqueous solution of $HAuCl_4$ (at a concentration of 10 mg/ml) was added at mass ratios of HA to $HAuCl_4$ from 1:1 to 1:0.1, respectively. The reaction mixtures were heated and stirred at 90 °C for 2 hours. Then, they were cooled to room temperature and stirred at room temperature for 12 hours.

Characterization of AuNPs

The microstructure of the samples was studied using scanning electron microscopy (SEM) and bright-field scanning transmission electron microscopy (BF-STEM) on a Hitachi Regulus 8220 electron microscope (Japan). Before measurements the samples were deposited on the 3 mm carbon-coated copper grids from water suspension. Images were acquired in transmitted electron mode at 30 kV accelerating voltage.

XPS spectra were obtained using a JEOL JPS 9010MX spectrometer (Japan) equipped with an X-ray source (Mg Kα). The pressure in the analytical chamber during spectrum acquisition was less than $7 \cdot 10^{-8}$ Pa. The samples of AuNP solutions were deposited on a titanium plates (Grade 4), and then dried from the solvent. Spectra were collected from 0 to 1100 eV with a pass energy of 50 eV and a step size of 0.5 eV. Binding energies (BE) were corrected by adjusting the position of the C1s peak to 284.7 eV. The JEOL SpecSurf software was used to determine peak areas, calculate elemental composition from peaks, and fit peaks to high-resolution spectra. Deconvolution of the spectra was performed using the Voigt function with the JEOL SpecSurf v. 1.9.0 software.

Optical properties of AuNPs solutions were determined by scanning all samples at 250 nm to 800 nm using UV–Vis spectrophotometer UV-1800 (Shimadzu, Japan).

The particle size distribution was studied by the means of Photon Cross-correlation Spectroscopy (PCCS) implemented in the NanoPhox (Sympatec, Germany). Particle size analysis was performed using the PAQXOS 4.2 program. Each sample was measured three times at 25 °C.

 doi:10.20944/preprints202510.0506.v1

Nanosphere™ Size Standards (ThermoFisher Scientific) with particle sizes 23±2, 100 and 510±7 nm were examined prior to analysis to verify the accuracy.

The SMH ζ-potential was measured by the optical heterodyning technique, using Zetasizer Nano ZS (Malvern Instruments Ltd., UK). In this technique, laser radiation scattering is used to measure the velocity of charged particles in an electric field applied to a cell through a pair of electrodes.

4. Conclusions

In this study, we have demonstrated the synthesis of gold nanoparticles using thiolated hyaluronic acid (HA-SH) as a synthetic and stabilization agent. A series of gold nanoparticles (**HA-AuNP1-4**) were synthesized by varying the mass ratio of HA-SH to $HAuCl_4$. The concentration of the gold precursor was found to be a critical parameter, directly influencing the size, morphology, and optical properties of the resulting AuNPs, as evidenced by UV-Vis, PCCS, SEM, and STEM analyses.

The investigation revealed that the reaction involves not only the reduction of Au^{3+} to form nanoparticles but also a concurrent chemical transformation of the thiol group. Comprehensive NMR and XPS analyses confirmed the oxidation of the thiol (-SH) groups to sulfonic acid ($-SO_3H$), suggesting a complex redox process alongside nanoparticle formation. Nevertheless, XPS analysis confirmed the metallic nature of the gold core (Au^0) and the presence of a Au-S bond, proving the direct involvement of the thiolated polymer in capping the nanoparticles.

The synthesized AuNPs were effectively stabilized by the anionic hyaluronic acid shell, as indicated by negative zeta potential values and SEM images.

In conclusion, thiolated hyaluronic acid serves as an effective platform for the one-pot synthesis and stabilization of gold nanoparticles with controllable characteristics. The unveiled oxidation pathway adds a new dimension to the understanding of the synthesis mechanism. The resulting HA-AuNPs, with their tunable properties represent promising candidates for further development in targeted drug delivery, theranostics, and other biomedical applications.

Supplementary Materials: The following supporting information can be downloaded at the website of this paper posted on Preprints.org, Figure S1: PCCS of HA-AuNP1 obtained in mass ratio system [2]:[$HAuCl_4$]=1:0.25; Figure S2: PCCS of HA-AuNP2 obtained in mass ratio system [2]:[$HAuCl_4$]=1:0.25; Figure S3: PCCS of HA-AuNP3 obtained in mass ratio system [2]:[$HAuCl_4$]=1:0.225; Figure S4: BF-STEM and SEM images of HA-AuNP1; Figure S5: BF-STEM and SEM images of HA-AuNP2; Figure S6: BF-STEM and SEM images of HA-AuNP3; Figure S7: NMR ^1H spectra of compound 2; Figure S8: NMR ^{13}C spectra of compound 2; Figure S9: NMR 2D COSY HH spectra of compound 2; Figure S10: NMR 2D HSQC spectra of compound 2; Figure S11: NMR ^1H spectra of the reaction mixture of 2 with $HAuCl_4$ at a ratio of [2]:[$HAuCl_4$]= 1:1; Figure S12: NMR ^{13}C spectra of the reaction mixture of 2 with $HAuCl_4$ at a ratio of [2]:[$HAuCl_4$]= 1:1; Figure S13: NMR 2D COSY HH spectra the reaction mixture of 2 with $HAuCl_4$ at a ratio of [2]:[$HAuCl_4$]= 1:1; Figure S14: NMR 2D HSQC spectra the reaction mixture of 2 with $HAuCl_4$ at a ratio of [2]:[$HAuCl_4$]= 1:1.

Author Contributions: Conceptualization, L.V.P.; methodology, Z.R.G., S.N.S, C.S.; formal analysis, Z.R.G., N.V.P.; investigation, E.I.A., G.U.G., Z.R.G., E.S.M., S.N.S., N.V.P.; resources, L.V.P., L.M.K., C.S.; data curation, E.I.A., G.U.G., Z.R.G., S.N.S., N.V.P.; writing—original draft preparation, E.I.A., G.U.G., E.S.M.; writing—review and editing, L.V.P., C.S.; visualization, E.I.A., G.U.G., E.S.M.; supervision, L.V.P.; project administration, L.M.K.; funding acquisition, L.M.K. All authors have read and agreed to the published version of the manuscript.

Funding: This work was financially supported by the Russian Science Foundation, grant number 23-73-00024, https://rscf.ru/project/23-73-00024.

Institutional Review Board Statement: Not applicable.

Informed Consent Statement: Not applicable.

Data Availability Statement: The datasets generated during and/or analyzed during the current study are available from the corresponding author on reasonable request.

 doi:10.20944/preprints202510.0506.v1

Conflicts of Interest: The authors declare no competing interests.

References

1. Hossain, A.; Rayhan, M.T.; Mobarak, M.H.; Rimon, M.I.H.; Hossain, N.; Islam, S.; Kafi, S.M.A.A. Advances and significances of gold nanoparticles in cancer treatment: A comprehensive review. *Results in Chemistry* **2024**, *8*, 101559, doi:https://doi.org/10.1016/j.rechem.2024.101559.
2. Shevtsov, M.; Zhou, Y.; Khachatryan, W.; Multhoff, G.; Gao, H. Recent Advances in Gold Nanoformulations for Cancer Therapy. *Curr Drug Metab* **2018**, *19*, 768-780, doi:https://doi.org/10.2174/1389200219666180611080736.
3. Abu-Dief, A.; Salaheldeen, M.; El-Dabea, T. Recent Advances in Development of Gold Nanoparticles for Drug Delivery Systems. *Journal of Modern Nanotechnology* **2021**, *1*, doi:http://dx.doi.org/10.53964/jmn.2021001.
4. Love, J.C.; Estroff, L.A.; Kriebel, J.K.; Nuzzo, R.G.; Whitesides, G.M. Self-Assembled Monolayers of Thiolates on Metals as a Form of Nanotechnology. *Chemical Reviews* **2005**, *105*, 1103-1170, doi:https://doi.org/10.1021/cr0300789.
5. Corma, A.; Garcia, H. Supported gold nanoparticles as catalysts for organic reactions. *Chemical Society Reviews* **2008**, *37*, 2096-2126, doi:https://doi.org/10.1039/B707314N.
6. Amendola, V.; Pilot, R.; Frasconi, M.; Maragò, O.M.; Iatì, M.A. Surface plasmon resonance in gold nanoparticles: a review. *J Phys Condens Matter* **2017**, *29*, 203002, doi:https://doi.org/10.1088/1361-648x/aa60f3.
7. Sergievskaya, A.; Chauvin, A.; Konstantinidis, S. Sputtering onto liquids: a critical review. *Beilstein J Nanotechnol* **2022**, *13*, 10-53, doi:https://doi.org/10.3762/bjnano.13.2.
8. Yang, X.; Shi, X.; D'Arcy, R.; Tirelli, N.; Zhai, G. Amphiphilic polysaccharides as building blocks for self-assembled nanosystems: molecular design and application in cancer and inflammatory diseases. *Journal of Controlled Release* **2018**, *272*, 114-144, doi:https://doi.org/10.1016/j.jconrel.2017.12.033.
9. Facchi, D.P.; da Cruz, J.A.; Bonafé, E.G.; Pereira, A.G.B.; Fajardo, A.R.; Venter, S.A.S.; Monteiro, J.P.; Muniz, E.C.; Martins, A.F. Polysaccharide-Based Materials Associated with or Coordinated to Gold Nanoparticles: Synthesis and Medical Application. *Curr Med Chem* **2017**, *24*, 2701-2735, doi:https://doi.org/10.2174/0929867324666170309123351.
10. Thodikayil, A.T.; Sharma, S.; Saha, S. Engineering Carbohydrate-Based Particles for Biomedical Applications: Strategies to Construct and Modify. *ACS Applied Bio Materials* **2021**, *4*, 2907-2940, doi:https://doi.org/10.1021/acsabm.0c01656.
11. Liu, H.; Zhang, M.; Meng, F.; Su, C.; Li, J. Polysaccharide-based gold nanomaterials: Synthesis mechanism, polysaccharide structure-effect, and anticancer activity. *Carbohydrate Polymers* **2023**, *321*, 121284, doi:https://doi.org/10.1016/j.carbpol.2023.121284.
12. Cai, Z.; Zhang, H.; Wei, Y.; Cong, F. Hyaluronan-Inorganic Nanohybrid Materials for Biomedical Applications. *Biomacromolecules* **2017**, *18*, 1677-1696, doi:https://doi.org/10.1021/acs.biomac.7b00424.
13. Cao, F.; Yan, M.; Liu, Y.; Liu, L.; Ma, G. Photothermally Controlled MHC Class I Restricted CD8+ T-Cell Responses Elicited by Hyaluronic Acid Decorated Gold Nanoparticles as a Vaccine for Cancer Immunotherapy. *Advanced Healthcare Materials* **2018**, *7*, 1701439, doi:https://doi.org/10.1002/adhm.201701439.
14. Skardal, A.; Zhang, J.; McCoard, L.; Oottamasathien, S.; Prestwich, G.D. Dynamically Crosslinked Gold Nanoparticle – Hyaluronan Hydrogels. *Advanced Materials* **2010**, *22*, 4736-4740, doi:https://doi.org/10.1002/adma.201001436.
15. Lin, C.-M.; Kao, W.-C.; Yeh, C.-A.; Chen, H.-J.; Lin, S.-Z.; Hsieh, H.-H.; Sun, W.-S.; Chang, C.-H.; Hung, H.-S. Hyaluronic acid-fabricated nanogold delivery of the inhibitor of apoptosis protein-2 siRNAs inhibits benzo[a]pyrene-induced oncogenic properties of lung cancer A549 cells. *Nanotechnology* **2015**, *26*, 105101, doi:https://doi.org/10.1088/0957-4484/26/10/105101.
16. Sanfilippo, V.; Caruso, V.C.; Cucci, L.M.; Inturri, R.; Vaccaro, S.; Satriano, C. Hyaluronan-Metal Gold Nanoparticle Hybrids for Targeted Tumor Cell Therapy. *International Journal of Molecular Sciences* **2020**, *21*, doi:https://doi.org/10.3390/ijms21093085.

 doi:10.20944/preprints202510.0506.v1

17. Kumar, C.S.; Raja, M.D.; Sundar, D.S.; Gover Antoniraj, M.; Ruckmani, K. Hyaluronic acid co-functionalized gold nanoparticle complex for the targeted delivery of metformin in the treatment of liver cancer (HepG2 cells). *Carbohydrate Polymers* **2015**, *128*, 63-74, doi:https://doi.org/10.1016/j.carbpol.2015.04.010.
18. Wang, J.; Liu, N.; Su, Q.; Lv, Y.; Yang, C.; Zhan, H. Green Synthesis of Gold Nanoparticles and Study of Their Inhibitory Effect on Bulk Cancer Cells and Cancer Stem Cells in Breast Carcinoma. *Nanomaterials* **2022**, *12*, doi:https://doi.org/10.3390/nano12193324.
19. Wang, W.; Li, D.; Zhang, Y.; Zhang, W.; Ma, P.; Wang, X.; Song, D.; Sun, Y. One-pot synthesis of hyaluronic acid–coated gold nanoparticles as SERS substrate for the determination of hyaluronidase activity. *Microchimica Acta* **2020**, *187*, 604, doi:https://doi.org/10.1007/s00604-020-04566-3.
20. Vávrová, A.; Čapková, T.; Kuřitka, I.; Vícha, J.; Münster, L. One-step synthesis of gold nanoparticles for catalysis and SERS applications using selectively dicarboxylated cellulose and hyaluronate. *International Journal of Biological Macromolecules* **2022**, *206*, 927-938, doi:https://doi.org/10.1016/j.ijbiomac.2022.03.043.
21. Lee, M.Y.; Yang, J.A.; Jung, H.S.; Beack, S.; Choi, J.E.; Hur, W.; Koo, H.; Kim, K.; Yoon, S.K.; Hahn, S.K. Hyaluronic acid-gold nanoparticle/interferon α complex for targeted treatment of hepatitis C virus infection. *ACS Nano* **2012**, *6*, 9522-9531, doi:https://doi.org/10.1021/nn302538y.
22. Kang, S.H.; Nafiujjaman, M.; Nurunnabi, M.; Li, L.; Khan, H.A.; Cho, K.J.; Huh, K.M.; Lee, Y.-k. Hybrid photoactive nanomaterial composed of gold nanoparticles, pheophorbide-A and hyaluronic acid as a targeted bimodal phototherapy. *Macromolecular Research* **2015**, *23*, 474-484, doi:https://doi.org/10.1007/s13233-015-3061-x.
23. Pouyani, T.; Prestwich, G.D. Functionalized Derivatives of Hyaluronic Acid Oligosaccharides: Drug Carriers and Novel Biomaterials. *Bioconjugate Chemistry* **1994**, *5*, 339-347, doi:https://doi.org/10.1021/bc00028a010.
24. Varghese, O.P.; Sun, W.; Hilborn, J.; Ossipov, D.A. In Situ Cross-Linkable High Molecular Weight Hyaluronan−Bisphosphonate Conjugate for Localized Delivery and Cell-Specific Targeting: A Hydrogel Linked Prodrug Approach. *Journal of the American Chemical Society* **2009**, *131*, 8781-8783, doi:https://doi.org/10.1021/ja902857b.
25. Henglein, A. Radiolytic Preparation of Ultrafine Colloidal Gold Particles in Aqueous Solution: Optical Spectrum, Controlled Growth, and Some Chemical Reactions. *Langmuir* **1999**, *15*, 6738-6744, doi:https://doi.org/10.1021/la9901579.
26. Boisselier, E.; Astruc, D. Gold nanoparticles in nanomedicine: preparations, imaging, diagnostics, therapies and toxicity. *Chemical Society Reviews* **2009**, *38*, 1759-1782, doi:https://doi.org/10.1039/b806051g.
27. Hien, N.Q.; Van Phu, D.; Duy, N.N.; Quoc, L.A. Radiation synthesis and characterization of hyaluronan capped gold nanoparticles. *Carbohydrate Polymers* **2012**, *89*, 537-541, doi:https://doi.org/10.1016/j.carbpol.2012.03.041.
28. Meen, T.-H.; Tsai, J.-K.; Chao, S.-M.; Lin, Y.-C.; Wu, T.-C.; Chang, T.-Y.; Ji, L.-W.; Water, W.; Chen, W.-R.; Tang, I.T.; et al. Surface plasma resonant effect of gold nanoparticles on the photoelectrodes of dye-sensitized solar cells. *Nanoscale Research Letters* **2013**, *8*, 450, doi:https://doi.org/10.1186/1556-276X-8-450.
29. Nyholm, R.; Berndtsson, A.; Martensson, N. Core level binding energies for the elements Hf to Bi (Z=72-83). *Journal of Physics C: Solid State Physics* **1980**, *13*, L1091, doi:10.1088/0022-3719/13/36/009.
30. Moulder, J.F.; Chastain, J.; King, R.C. *Handbook of X-ray Photoelectron Spectroscopy: A Reference Book of Standard Spectra for Identification and Interpretation of XPS Data*; Physical Electronics: 1995.
31. Casaletto, M.P.; Longo, A.; Martorana, A.; Prestianni, A.; Venezia, A.M. XPS study of supported gold catalysts: the role of Au0 and Au+δ species as active sites. *Surface and Interface Analysis* **2006**, *38*, 215-218, doi:https://doi.org/10.1002/sia.2180.
32. Sahoo, S.R.; Ke, S.-C. Spin-Orbit Coupling Effects in Au 4f Core-Level Electronic Structures in Supported Low-Dimensional Gold Nanoparticles. *Nanomaterials* **2021**, *11*, 554, doi:https://doi.org/10.3390/nano11020554.
33. Eatoo, M.A.; Wehbe, N.; Kharbatia, N.; Guo, X.; Mishra, H. Why do some metal ions spontaneously form nanoparticles in water microdroplets? Disentangling the contributions of the air–water interface and bulk redox chemistry. *Chemical Science* **2025**, *16*, 1115-1125, doi:https://doi.org/10.1039/D4SC03217A.

 doi:10.20944/preprints202510.0506.v1

34. Wang, K.; Liu, Q. Adsorption of phosphorylated chitosan on mineral surfaces. *Colloids and Surfaces A: Physicochemical and Engineering Aspects* **2013**, *436*, 656-663, doi:https://doi.org/10.1016/j.colsurfa.2013.07.030.
35. Rouxhet, P.G.; Genet, M.J. XPS analysis of bio-organic systems. *Surface and Interface Analysis* **2011**, *43*, 1453-1470, doi:https://doi.org/10.1002/sia.3831.
36. Fan, C.; Chen, C.; Wang, J.; Fu, X.; Ren, Z.; Qian, G.; Wang, Z. Black Hydroxylated Titanium Dioxide Prepared via Ultrasonication with Enhanced Photocatalytic Activity. *Scientific Reports* **2015**, *5*, 11712, doi:https://doi.org/10.1038/srep11712.
37. Castner, D.G.; Hinds, K.; Grainger, D.W. X-ray Photoelectron Spectroscopy Sulfur 2p Study of Organic Thiol and Disulfide Binding Interactions with Gold Surfaces. *Langmuir* **1996**, *12*, 5083-5086, doi:https://doi.org/10.1021/la960465w.
38. Lindberg, B.J.; Hamrin, K.; Johansson, G.; Gelius, U.; Fahlman, A.; Nordling, C.; Siegbahn, K. Molecular Spectroscopy by Means of ESCA II. Sulfur compounds. Correlation of electron binding energy with structure. *Physica Scripta* **1970**, *1*, 286, doi:10.1088/0031-8949/1/5-6/020.
39. Shanthi, P.M.; Hanumantha, P.J.; Ramalinga, K.; Gattu, B.; Datta, M.K.; Kumta, P.N. Sulfonic Acid Based Complex Framework Materials (CFM): Nanostructured Polysulfide Immobilization Systems for Rechargeable Lithium–Sulfur Battery. *Journal of The Electrochemical Society* **2019**, *166*, A1827, doi:http://dx.doi.org/10.1149/2.0251910jes.
40. Zhang, Q.; Tao, Q.; He, H.; Liu, H.; Komarneni, S. An efficient SO2-adsorbent from calcination of natural magnesite. *Ceramics International* **2017**, *43*, 12557-12562, doi:https://doi.org/10.1016/j.ceramint.2017.06.130.
41. Tudino, T.C.; Nunes, R.S.; Mandelli, D.; Carvalho, W.A. Influence of Dimethylsulfoxide and Dioxygen in the Fructose Conversion to 5-Hydroxymethylfurfural Mediated by Glycerol's Acidic Carbon. *Frontiers in Chemistry* **2020**, *Volume 8 - 2020*, doi:https://doi.org/10.3389/fchem.2020.00263.
42. Shu, X.Z.; Liu, Y.; Luo, Y.; Roberts, M.C.; Prestwich, G.D. Disulfide Cross-Linked Hyaluronan Hydrogels. *Biomacromolecules* **2002**, *3*, 1304-1311, doi:https://doi.org/10.1021/bm025603c.
43. Reich, H.J. Organic Chemistry Data Collection. Available online: https://organicchemistrydata.org/hansreich/resources/nmr/?page=05-hmr-15-aabb%2F (accessed on 09/01/2020).
44. Herke, R.; Rasheed, K. Addition of bisulfite to α-olefins: Synthesis of n-alkane sulfonates and characterization of intermediates. *Journal of the American Oil Chemists Society* **1992**, *69*, 47-51, doi:https://doi.org/10.1007/BF02635876.
45. He, R.; Wang, J.; Yu, Z.-H.; Moyers, J.S.; Michael, M.D.; Durham, T.B.; Cramer, J.W.; Qian, Y.; Lin, A.; Wu, L.; et al. Structure-Based Design of Active-Site-Directed, Highly Potent, Selective, and Orally Bioavailable Low-Molecular-Weight Protein Tyrosine Phosphatase Inhibitors. *Journal of Medicinal Chemistry* **2022**, *65*, 13892-13909, doi:https://doi.org/10.1021/acs.jmedchem.2c01143.
46. Witt, D. Recent Developments in Disulfide Bond Formation. *Synthesis* **2008**, *2008*, 2491-2509, doi:http://dx.doi.org/10.1055/s-2008-1067188.
47. McNeil, N.M.R.; McDonnell, C.; Hambrook, M.; Back, T.G. Oxidation of Disulfides to Thiolsulfinates with Hydrogen Peroxide and a Cyclic Seleninate Ester Catalyst. *Molecules* **2015**, *20*, 10748-10762, doi:https://doi.org/10.3390/molecules200610748.
48. Spiliopoulou, N.; Kokotos, C.G. Photochemical metal-free aerobic oxidation of thiols to disulfides. *Green Chemistry* **2021**, *23*, 546-551, doi:https://doi.org/10.1039/D0GC03818K.
49. Koval, I.V. The chemistry of disulfides. *Russian Chemical Reviews* **1994**, *63*, 735, doi:10.1070/RC1994v063n09ABEH000115.
50. Bagiyan, G.A.; Koroleva, I.K.; Soroka, N.V.; Ufimtsev, A.V. Oxidation of thiol compounds by molecular oxygen in aqueous solutions. *Russian Chemical Bulletin* **2003**, *52*, 1135-1141, doi:https://doi.org/10.1023/A:1024761324710.
51. van Bergen, L.A.H.; Roos, G.; De Proft, F. From Thiol to Sulfonic Acid: Modeling the Oxidation Pathway of Protein Thiols by Hydrogen Peroxide. *The Journal of Physical Chemistry A* **2014**, *118*, 6078-6084, doi:https://doi.org/10.1021/jp5018339.

 doi:10.20944/preprints202510.0506.v1

52. Lunardi, C.N.; Gomes, A.J.; Rocha, F.S.; De Tommaso, J.; Patience, G.S. Experimental methods in chemical engineering: Zeta potential. *The Canadian Journal of Chemical Engineering* **2021**, *99*, 627-639, doi:https://doi.org/10.1002/cjce.23914.
53. Chauvin, J.-P.R.; Pratt, D.A. On the Reactions of Thiols, Sulfenic Acids, and Sulfinic Acids with Hydrogen Peroxide. *Angewandte Chemie International Edition* **2017**, *56*, 6255-6259, doi:https://doi.org/10.1002/anie.201610402.
54. Vercruysse, K.P.; Marecak, D.M.; Marecek, J.F.; Prestwich, G.D. Synthesis and in Vitro Degradation of New Polyvalent Hydrazide Cross-Linked Hydrogels of Hyaluronic Acid. *Bioconjugate Chemistry* **1997**, *8*, 686-694, doi:https://doi.org/10.1021/bc9701095.